

# Attribution of SST variability in global oceans and the role of ENSO

Arun Kumar · Bhaskar Jha · Hui Wang

Received: 26 February 2013 / Accepted: 1 July 2013 / Published online: 14 July 2013  
© Springer-Verlag (outside the USA) 2013

**Abstract** Based on a novel design of coupled model simulations where sea surface temperature (SST) variability in the equatorial tropical Pacific was constrained to follow the observed El Niño—Southern Oscillation (ENSO) variability, while rest of the global oceans were free to evolve, the ENSO response in SSTs over the other ocean basins was analyzed. Conceptually the experimental setup was similar to discerning the contribution of ENSO variability to interannual variations in atmospheric anomalies. A unique feature of the analysis was that it was not constrained by a priori assumptions on the nature of the teleconnected response in SSTs. The analysis demonstrated that the time lag between ENSO SST and SSTs in other ocean basins was about 6 months. A signal-to-noise analysis indicated that between 25 and 50 % of monthly mean SST variance over certain ocean basins can be attributed to SST variability over the equatorial tropical Pacific. The experimental setup provides a basis for (a) attribution of SST variability in global oceans to ENSO variability, (b) a method for separating the ENSO influence in SST variations, and (c) understanding the contribution from other external factors responsible for variations in SSTs, for example, changes in atmospheric composition, volcanic aerosols, etc.

## 1 Introduction

Attribution of climate anomalies is an important aspect of improving our understanding of causes for climate variability with potential for improving long-range predictions. Indeed, it was the discovery of global atmospheric teleconnections related to the tropical Pacific sea surface temperature (SST) variability associated with the El Niño—Southern Oscillation (ENSO) (Horel and Wallace 1981) that bolstered the justification for the seasonal prediction efforts. Identification of the importance of ENSO SST variability on global climate was the primary impetus for the establishment of Tropical Atmosphere Global Atmosphere (TOGA) program to better understand and predict ENSO variability, culminating in the deployment of TAO/TRITON array in the equatorial tropical Pacific (McPhaden et al. 2010) and development of dynamical seasonal prediction systems (Ji et al. 1994; Stockdale et al. 1998).

Extensive work followed the initial analysis of Horel and Wallace (1981) to develop theoretical underpinnings for global teleconnections related to the ENSO SST variability, and to better understand various nuances of this relationship, e.g., non-linearity (Hoerling et al. 1997), delayed atmospheric response (Kumar and Hoerling 2003), and response to different favors of ENSO, etc. (Trenberth et al. 1998; Kumar and Hoerling 1997). To overcome sampling issues due to the limited observational record, much of the latter advancements relied on ensembles of atmospheric general circulation model simulations forced with the evolution of the observed SSTs (the so called AMIP simulations). Availability of ensemble of AGCM simulations provided a unique methodology to identify the atmospheric response patterns associated with the interannual SST variability.

Subsequent research efforts also revealed that ENSO SST variability not only affects the atmospheric climate

---

A. Kumar (✉) · B. Jha · H. Wang  
Climate Prediction Center, NOAA/NWS/NCEP,  
5830 University Research Court, NCWCP, College Park,  
MD, USA  
e-mail: arun.kumar@noaa.gov

B. Jha · H. Wang  
WYLE, Science, Technology and Engineering Group,  
Houston, TX, USA

variability but also the SST variability in the other ocean basins (Jones 1988; Klein et al. 1999; Kumar and Hoerling 2003; Chiang and Lintner 2005; Chang et al. 2006). This connection between the SST variability in the equatorial tropical Pacific and other oceans is mediated via the atmospheric bridge (Lau and Nath 1996; Alexander et al. 2002) as the time scale of oceanic pathways is much longer than the time-scale of ENSO variability, except over the region of Indonesian through flow (England and Huang 2005). However, to identify to what extent the interannual SST variability in ocean basins other than equatorial tropical Pacific can be attributed to ENSO SST variability remains an area of ongoing research, particularly for determining the possible influence of various simplifying assumptions on conclusions as discussed below.

The simplest approach to identify the teleconnected variability between ENSO-related SST and SSTs in other ocean basins is based on linear analysis where an index of ENSO SST (for example, Niño 3.4 SST index (Barnston et al. 1997) or the principal component of the leading EOF of SST variability in the tropical Pacific related to ENSO) is regressed against the global SST variability. This analysis can easily be done based on the historical SST data (Lanzante 1996; Klein et al. 1999). The next step in complexity of the analysis, which is not constrained by the assumption of linearity, is to develop simultaneous composites of global SST anomalies related to warm and cold phases of ENSO. These analyses led to the identification of the horseshoe pattern of opposite sign SST anomalies straddling the primary ENSO-related SST in the equatorial Pacific (Lanzante 1996); a signal in SST anomalies in the extratropical Pacific that projects on the spatial structure of the SST related to the Pacific decadal oscillation (PDO) (Newman et al. 2003); and in phase SST anomalies in the tropical Indian and Atlantic basins (Barnston 1994; Goddard and Graham 1999; Chang et al. 2006).

One of the shortcomings of linear, or of the compositing approach, however is that as the SST response in global oceans to ENSO SST tends to be delayed by several months because of thermal inertia of the oceans (with lag varying from one ocean basin to another) (Klein et al. 1999; Kumar and Hoerling 2003), this response cannot be well captured by aforementioned techniques. Various statistical approaches have been developed to account for this lagged relationship (Chen et al. 2008; Compo and Sardeshmukh 2010), but these methods are still variants of linear approaches and cannot take into account potential non-linearity in the SST response.

A full understanding of the relationship between ENSO SST and SST variability in other ocean basins that takes into account the delayed response, and other potential non-linear aspects in the response, is important in several contexts. For example, on the interannual time-scale, the

variability of surface and tropospheric temperatures is highly constrained by the ENSO variability (Kumar et al. 2004). From the perspective of understanding and attributing temperature and precipitation trends due to the anthropogenic causes, removal of ENSO related signal is desired (Kelly and Jones 1996; Kumar et al. 2004). In another example, ENSO related SST variability in other ocean basins also represents a predictable component of SSTs due to ENSO (to the extent ENSO SST variability itself can be predicted), and therefore, identification of this signal represents the predictability of SST that is potentially predictable, and needs to be correctly simulated in climate models.

In this analysis, we report on an ensemble based approach where, in a coupled model simulation, the SST variability in the equatorial tropical Pacific is constrained to follow the observed variability, while the SSTs in other ocean basins are free to evolve. The design of model simulation with a fully coupled ocean–atmosphere evolution in ocean basins other than equatorial tropical Pacific extends on simulations done with ocean mixed layer models (Alexander and Scott 2002; Lau and Nath 2003), or experiments for a specific case of ENSO (Elliott et al. 2001), or with coupling over the region of interest, for example, Indian Ocean (Huang and Shukla 2007) or Atlantic Ocean (Huang 2004) but with observed SSTs specified over all other ocean basins.

Based on the analysis of the ensemble mean of simulations we infer the ENSO-related SST signal in other ocean basins. The approach follows the analysis of variance method for the seasonal atmospheric variability forced by SSTs and has been widely used (Kumar and Hoerling 1995; Rowell 1998; Peng et al. 2000). Further, the analysis approach is not constrained by any a priori assumption (for example, linearity or specifying the time lag for the delayed response); however, results could be influenced by the biases in the coupled model used in our simulations.

The paper describes the design of the coupled model simulations (Sect. 2). The analysis approach follows decomposing the variability of SST into one component related to ensemble mean (and is due to ENSO), and one that related to the departure from the ensemble mean (i.e., due to internal variations (Sect. 3)). The paper concludes with a summary and assessment of SST predictability related to ENSO (Sect. 4).

## 2 Data and coupled model simulation

The coupled model used in this study is the early version of the Climate Forecast System (CFS; Saha et al. 2006) that was implemented for operational seasonal forecast at the National Centers for Environmental Prediction (NCEP) during 2004–2012. The atmospheric, oceanic, and land

components of the coupled model are the NCEP Global Forecast System (GFS) version 1 (Moorthi et al. 2001), the Geophysical Fluid Dynamics Laboratory (GFDL) Modular Ocean Model version 3 (MOM3; Pacanowski and Griffies 1998), and the Oregon State University (OSU) land surface model (LSM; Pan and Mahrt 1987), respectively.

The atmospheric GFS has T62 horizontal resolution and 64 vertical levels. The GFDL MOM3 covers global oceans from 74°S to 64°N, with horizontal resolutions of 1° (longitude) by 1/3° (latitude) between 10°S and 10°N, and increasing to 1° (latitude) poleward of 30°S and 30°N. The MOM3 has 40 layers from 5 m below sea level to 4,479 m, with a 10-m resolution in the upper 240 m. The OSU LSM has two soil layers: 0–10 cm and 10–190 cm. More detailed descriptions of the CFS are given in Saha et al. (2006).

To constrain the coupled model responses to realistic ENSO variability, tropical Pacific SSTs in the coupled simulations are relaxed to the observed daily SST. This is done by replacing the model predicted SST in the tropical Pacific domain (10°S–10°N, 140°E–75°W) with new SST after each 1-day integration of the coupled model. The new SST ( $SST_{NEW}$ ) is a combination of the coupled model predicted SST ( $SST_{MOM3}$ ) and the observed daily SST ( $SST_{OBS}$ ) interpolated from the weekly OISST based on the following equation:

$$SST_{NEW} = (1 - w)SST_{MOM3} + wSST_{OBS},$$

where  $w$  is a weighting coefficient, which is set to 1/3 in the tropical Pacific domain (10°S–10°N, 140°E–75°W) and is linearly reduced to 0 on the border of an extended domain (15°S–15°N, 130°E–65°W). The value of 1/3, equivalent to nudging the model SST to the observed SST with a restoring timescale of 3.3 days, effectively constrains monthly mean  $SST_{NEW}$  in the tropical Pacific to the observations and thus ensures the realistic ENSO variability in the CFS. In the rest of global oceans  $w = 0$ , and the atmosphere and ocean remain fully coupled.

The modified CFS with relaxation of the model predicted SST to the observed SST in the tropical Pacific (indicated by TPCF in the figures) was integrated over the 31-year period (1981–2011) starting with one ocean initial condition but nine different atmospheric initial conditions. The ocean model was initialized with 1 January 1981 condition obtained from the NCEP Global Ocean Data Assimilation System (GODAS; Behringer and Xue 2004). The atmospheric model was initialized with 28 December 1980 to 5 January 1981 conditions, each one day apart, obtained from the NCEP/Department of Energy (DOE) Global Reanalysis 2 (R2; Kanamitsu et al. 2002). This procedure results in an ensemble of nine member simulations in which the SST variability in equatorial tropical Pacific follows the observed evolution, while SST variability in other ocean basins is a combination of internal

variability and external variability forced by ENSO. The model simulations for the 1983–2010 period are used in the analysis. Results from these simulations have been reported in Chen et al. (2012).

For the observed SST variability over the global oceans, we used observation-based monthly mean analyses: version 2 of the optimum interpolation (OIv2) SST (Reynolds et al. 2002) at 2.5 × 2.5 degree grid.

### 3 Results

A comparison of monthly mean SST variability between observations and model simulation is shown in Fig. 1. This

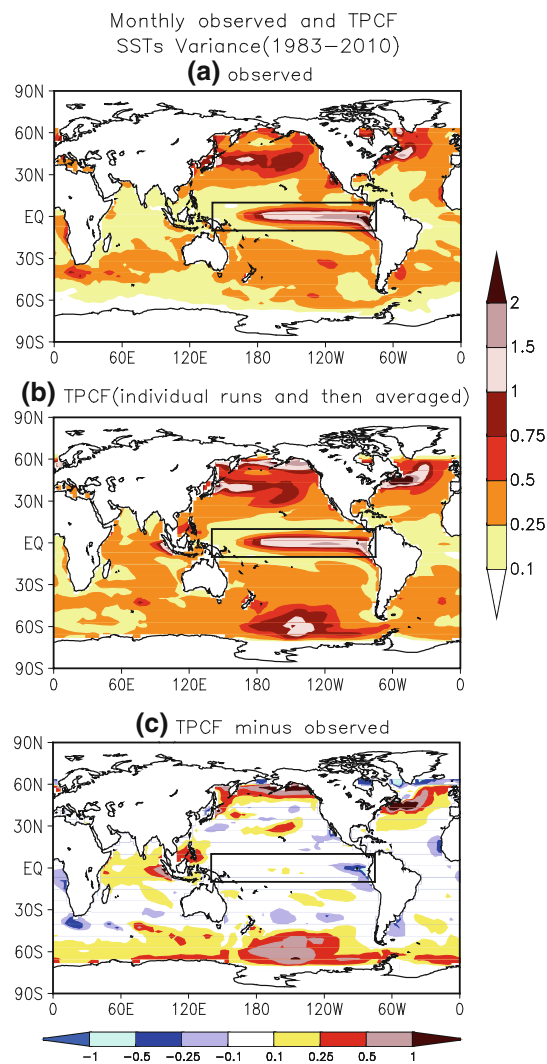


**Fig. 1** Variance of monthly mean SSTs for **a** observations, **b** model simulations (TPCF), and **c** difference between model simulated and observed variance. Units are in °K<sup>2</sup>. For model simulations variance is obtained for each run and then averaged over estimates from nine runs. The box in the equatorial tropical Pacific indicates the spatial domain over which the predicted SSTs are merged with the observed evolution of SSTs

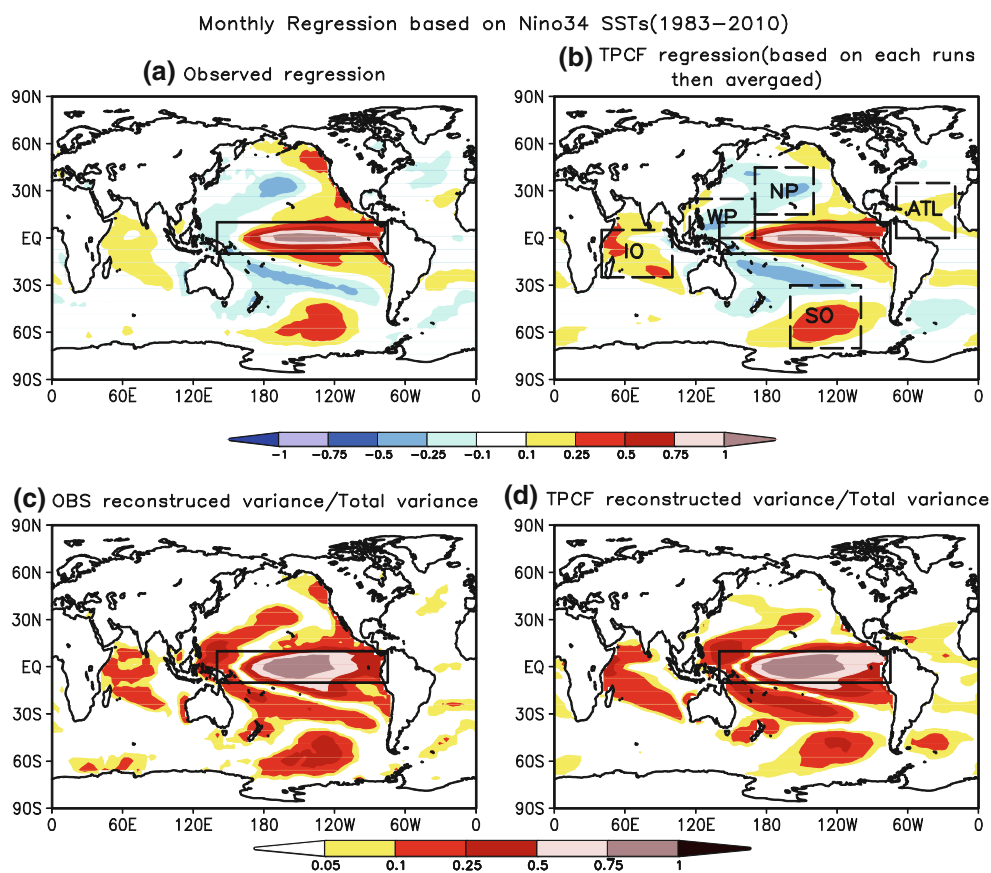


**Fig. 2** (Top row) Spatial pattern of regression between monthly mean SST variability and Niño 3.4 SST index for **a** observations, and **b** model simulations. Units are in °K. For model simulations, regression is obtained for each run and then averaged over estimates from nine runs. (Bottom row) Ratio of reconstructed monthly mean variance of SST and total variance for **c** observations, and **d** model

simulations. The reconstruction is based on respective Niño 3.4 regression maps in the top row. The box in the equatorial tropical Pacific indicates the spatial domain over which the predicted SSTs are merged with the observed evolution of SSTs. Dashed boxes in top right panels are the spatial domains over which SSTs are averaged to analyze regional features

analysis provides a basic assessment of realism of SST variability in the model simulations. For the model, SST variability is first computed over individual simulations in the ensemble, and then averaged over nine simulations. For both observations and the model, results are shown averaged over all months.

For model simulations, the SST variability over the oceans where they are free to evolve has realistic amplitudes. The largest discrepancy in the tropical latitude occurs immediately to the west of Indonesia (a region corresponding to the eastern node of the Indian Ocean Dipole) where SST variability is overestimated. In the extratropics the largest errors are over the Gulf Stream (likely due to a coarse model resolution), and near the sea ice edges in the northern and southern hemisphere.

We next evaluate the component of the simultaneous monthly mean SST variability in the ocean basins other than the tropical Pacific that is linearly related to the ENSO variability. The first assessment is based on the regression with the Niño 3.4 SST index and results are shown in

Fig. 2 (top row). Once again, for the models regression is computed for individual model simulations, and the average of nine regression maps is shown.

The spatial pattern of the regression map is consistent with the well documented influence of ENSO variability in the tropical Pacific on the other ocean basins: a horseshoe pattern of opposite sign SST anomalies extending into extratropical latitudes; a spatial pattern in the North Pacific ocean that is similar to the SST fingerprint associated with the PDO; a tendency for positive SST regressions over the equatorial Indian and Atlantic Oceans signifying an in-phase relationship with the evolution of ENSO variability. There is very good spatial resemblance between observation and model simulation. The regression pattern also reveals the regions where SST variability is related to the remote ENSO SST variability via the atmospheric bridge mechanism (Lau and Nath 1996; Alexander et al. 2002).

An additional point to note is that the amplitude of the regression is also well simulated, and although there were discrepancies in the absolute value of the monthly mean SST

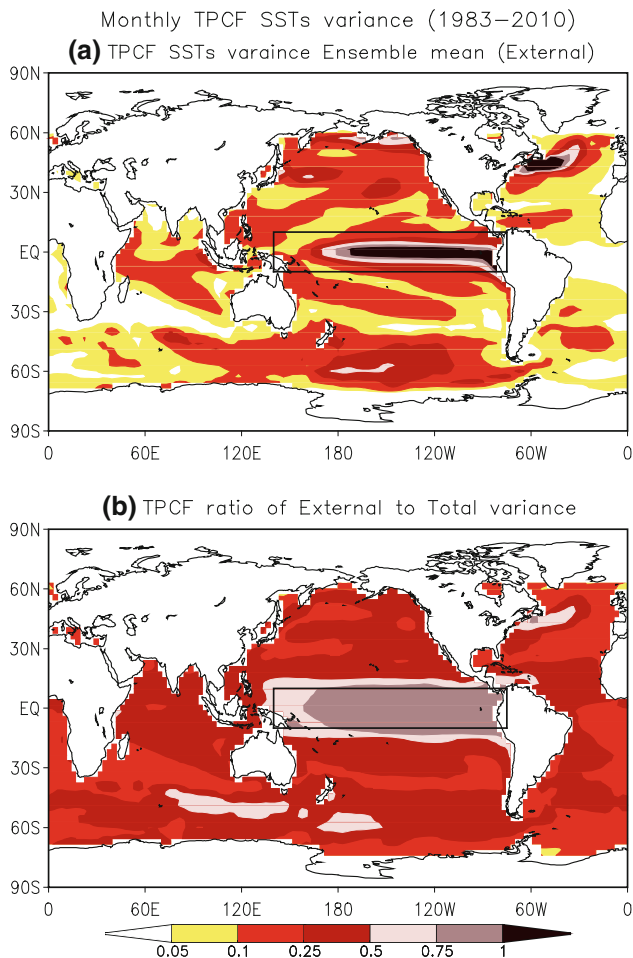


**Fig. 3** **a** Variance of monthly mean SSTs for the ensemble average of model simulations. Units are in  $^{\circ}\text{K}^2$ . **b** Ratio of variance of ensemble averaged monthly mean SSTs and total variance for model simulations. The *box* in the equatorial tropical Pacific indicates the spatial domain over which the predicted SSTs are merged with the observed evolution of SSTs

variability (Fig. 1), the relative amplitude of the fraction of variability related to ENSO has a very good match.

The signal-to-noise ratio (SNR) that can be linearly associated with the Niño 3.4 SST index variability is also shown in Fig. 2 (bottom panels). The SNR is computed as follows: (a) respective regression patterns in Fig. 2 (top panels) are used to first reconstruct the SST component that is linearly related to the Niño 3.4 SST index. This results in a monthly mean SST time series over the analysis period that is linearly related to ENSO; (b) variance of the reconstructed SST time-series then provides the component (or the signal) that is linearly related to the Niño 3.4 SST index; and finally (c) ratio of variance of the reconstructed SST to the variance of original SST (in Fig. 1) is defined as the SNR and is indicative of fraction of variance linearly explained by the variability in the Niño 3.4 SST index. SNR of 1 (0) means that entire (none of) the variability of SST can be related to Niño 3.4 SST index.

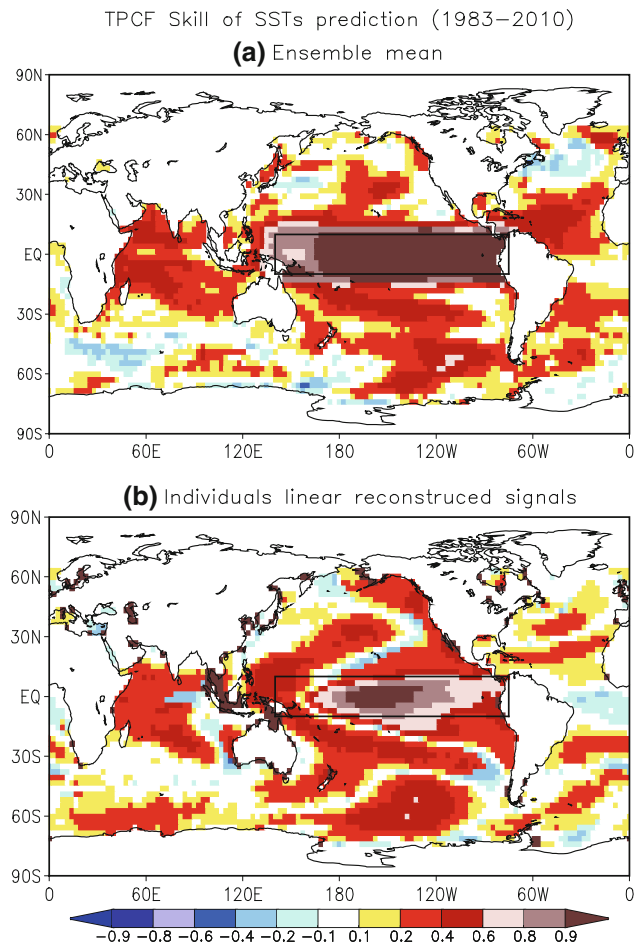


**Fig. 4** Anomaly correlation between monthly mean observed SSTs and model simulated SSTs for **a** when model simulated SST is based on ensemble mean, and **b** when model simulated SST is based on reconstruction using the regression pattern

Both for the observation and for the model, the fraction of monthly mean SST variability linearly related to the Niño 3.4 SST index is around 15–20 % with some regions exceeding 25 % (e.g., north of equator in western Pacific). Once again, there is a good correspondence both in the spatial pattern and the magnitude of the SNR between observation and the model.

The estimate of SNR shown in Fig. 2 is based on a simultaneous analysis, and further, is constrained by the assumption of linearity. For observations, because of the limited data record, a better estimate that can account for non-linear influences, or a delay in the oceanic response to ENSO variability, is confounded by sampling issues and is not feasible (Kumar and Hoerling 1997, 2000). Availability of ensemble of model simulations, however, allows us to explore the SNR beyond the assumption of linearity, and although the model based estimate cannot be validated directly against the observations, the resemblance for the case of the analysis under the assumption of linearity

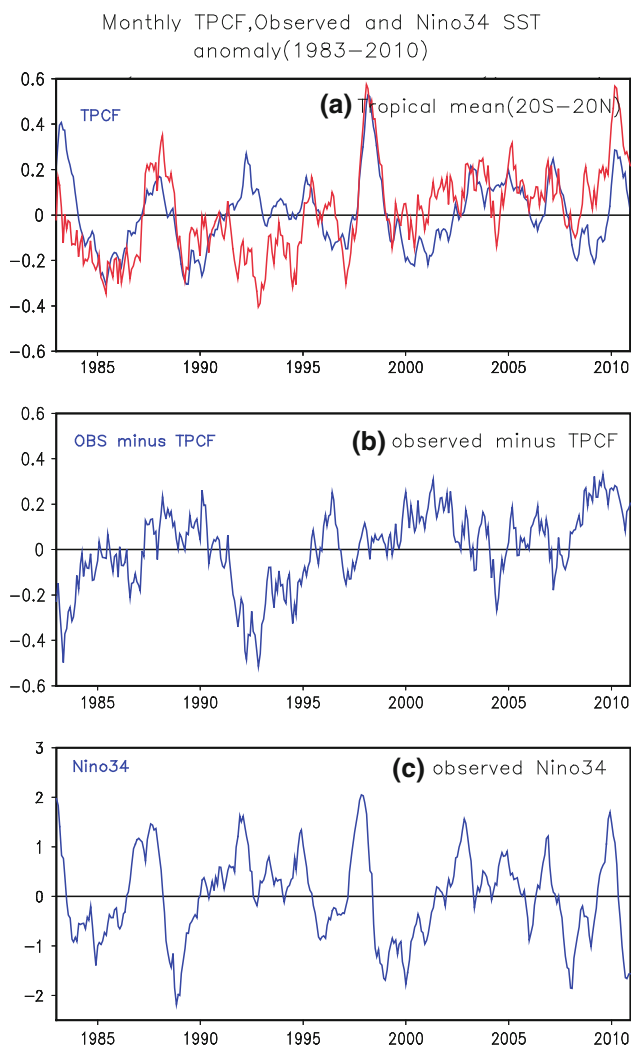


**Fig. 5** **a** Time evolution of tropical average of observed SSTs (*red curve*) and model simulated SSTs (*blue curve*). Domain of spatial average is from 20°S to 20°N and excludes the region where observed SST variability was specified. **b** Difference between observed and model simulated SSTs in the top panel. **c** Time evolution of observed Niño 3.4 SST Index. Units are in °K

(Fig. 2) between observation and model provides us with the confidence to pursue the model based approach further.

The analysis of SNR based on the ensemble of model simulations follows the approach similar to that for the traditional analysis for the atmospheric variability (Kumar and Hoerling 1995). Following this approach, variability in SST due to ENSO SST is computed based on the ensemble mean (a procedure that reduces the contribution of random component in the individual model runs towards the variability of ensemble mean). The variance of the ensemble mean of SST, together with the SNR is shown in Fig. 3. The variance of the ensemble mean can also be compared with the variance of linear reconstruction of SST based on the Niño 3.4 SST index.

The variance of ensemble mean SST (Fig. 3, top panel) that is due to the influence of ENSO on other ocean basins and this estimate, not constrained by the assumption of linearity and simultaneity, is generally larger than that based on the linear construction (not shown), indicating that a larger fraction of SST variability can be attributed to the SST variability in the tropical eastern Pacific. This is reflected further in the SNR (Fig. 3, bottom panel) that has larger positive SNR values than its linear counterpart (Fig. 2, bottom right).

The amplitude of the SNR is directly proportional to the skill of ensemble mean as the prediction (Kumar and Hoerling 2000) with higher (lower) SNR having higher (lower) prediction skill. For example, as measured by the anomaly correlation (AC), the skill of the SST prediction based on the ensemble mean (with higher SNR) should be better than the skill based on the linearly regressed SST signal related to the Niño 3.4 SST index. This comparison also provides a check in that if the SNR estimate based on ensemble of model simulations is high but the AC is not, it points to possible bias in model's simulation (and estimate) of the SNR.

The AC for SST forecasts based on ensemble mean and based on the reconstructed signal is shown in Fig. 4. The skill of SST forecast based on ensemble mean (Fig. 4, top panel) is generally better than the skill based on linearly reconstructed SST signal (Fig. 4, bottom panel). This is particularly true over the tropical Indian and Atlantic Oceans. This need not be the case if the SST signal based on the ensemble mean of the simulation is erroneous and does not reflect observed SST evolution. One such example is associated with the variability over the Gulf Stream where although the SNR estimate is very high, AC is negative, and in fact, is worse than for the regressed SST as prediction. Barring few exceptions, *a combination of a higher SNR accompanied by higher skill is an indication that the SST signal computed based on ensemble of runs is realistic and that the linear response to ENSO is an underestimation of the ENSO related signal in other ocean basins.*

We next analyze the monthly variability in the observed SST in tropical ocean basins other than the Pacific. The global tropical mean of SSTs averaged between the 20°S–20°N latitude band is shown in Fig. 5 (top panel). To see what fraction of observed variability is explained by the ENSO variability, the average of SST anomaly based on the ensemble average of the model simulations (i.e., the ENSO related signal) is also shown.

Consistent with earlier analysis (Kumar et al. 2004), there is a clear indication that the interannual variability in observed SSTs has a signature of the ENSO variability (which is shown as time series of Niño 3.4 SST index, Fig. 5, bottom panel) with a mean warming (cooling) in

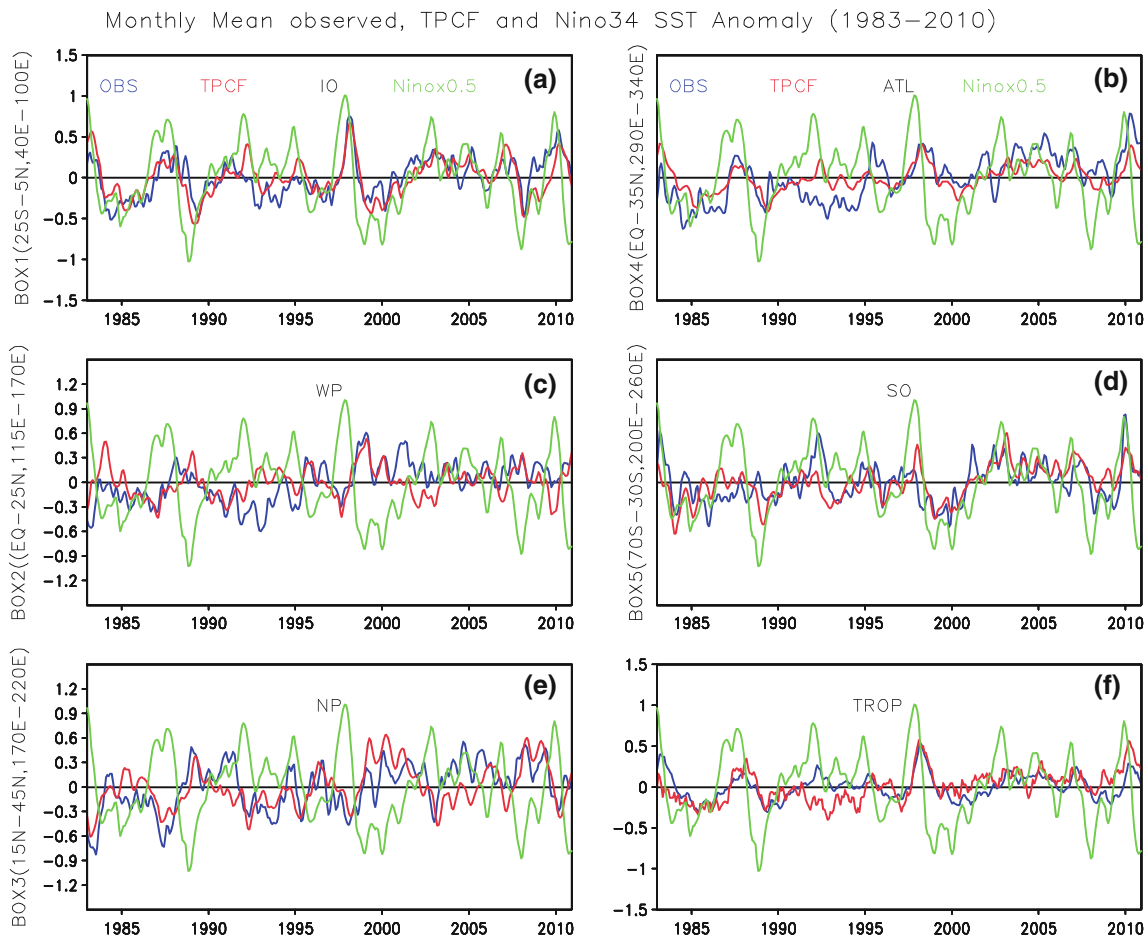


**Fig. 6** Time evolution of observed (blue curve) and model simulated (red curve) SST anomalies area averaged over different spatial domains: **a** Indian Ocean (IO); **b** Atlantic (ATL); **c** Western Pacific (WP); **d** Southern Oceans (SO); **e** North Pacific (NP), and **f** tropical

oceans (TROP). In all panels green curve is the Niño 3.4 SST index multiplied by factor 0.5. Panel **f** repeats the analysis shown in Fig. 5. Units are in °K. Areas covered by different boxes are indicated in Fig. 2

tropical ocean basins following El Niño (La Niña) events. The time-series of ensemble mean SST variability in the model simulation (with a few exceptions discussed later) closely follows the observed variability and indicates the control of tropical Pacific SST on the interannual variability in other ocean basins. From a comparison of the different time series—in the bottom panel for Niño 3.4 SST index, and top panel for the observations and ensemble mean simulated SST—it is apparent that the ENSO related SST signal in the other tropical oceans also lags the ENSO variability by several months. For different tropical and extratropical ocean basins, this aspect of lagged response will be discussed later.

The difference between the observed and model simulated SST time series (Fig. 5, middle panel) illustrates some notable discrepancies. One is a marked cooling in the observed SST time-series starting around 1982 and then again in 1992. This cooling is not replicated as an ensemble mean response to ENSO SSTs and is related to a general

cooling of tropical ocean basins due to volcanic eruptions (Stenchikov et al. 2009; Xue et al. 2012)—El Chichon in 1982 and Mount Pinotubo in 1991.

The other notable discrepancy is a slow rise in the observed temperature that is not replicated in the ensemble mean SST time series. This is related to the possibility that the warming in the other ocean basins is due to the changes in atmospheric composition—increases in the greenhouse gases (GHGs)—and is not related to the ENSO. It has been documented that although SSTs in other ocean basins have been getting warmer, SSTs in the tropical eastern Pacific have not experienced a similar trend (Kumar et al. 2010; L’Heureux et al. 2013). Therefore, due to lack of warming trends in specified SSTs in the equatorial Pacific, and the fact that model simulations are done with a fixed CO<sub>2</sub>, a trend in SST response in other ocean basins also does not exist.

We note that although the design of model simulations was to infer the ENSO related SST variability in different ocean basins, it is encouraging to see that influence of other

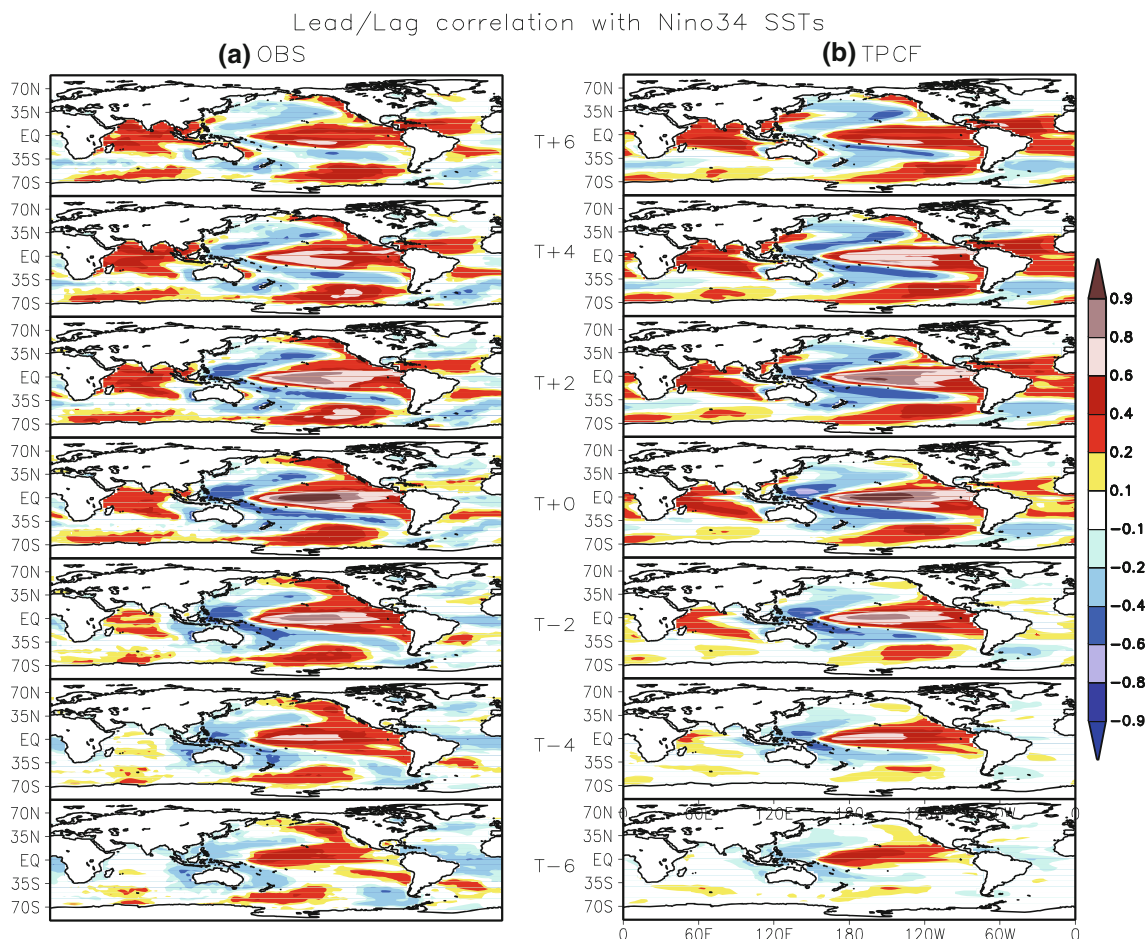


**Fig. 7** Lead–lag correlation between Niño3.4 SST index and **a** observed SSTs, and **b** model simulated SSTs. Rows from bottom to top are for Niño 3.4 SST index lagging (with months indicated by *negative integers*) or leading (with months indicated by *positive integers*)

extraneous causes (e.g., volcanoes, or changes in the GHGs), and their signal on SST variability, can also be gleaned. Further, the method of removal of ENSO time series is not constrained by any a priori assumptions (e.g., linearity, or what is the time lag for the SST response), however, the analysis could be influenced by model biases that may affect the SST response to ENSO in other ocean basins.

We next analyze the interannual variations in the SST in different ocean basins, and to the extent observed variations are linked to ENSO variability. Time series of the observed and the ensemble mean SST evolution for model simulations, area averaged over different oceanic regions, is shown in Fig. 6, and the respective ocean basins are marked by boxes in Fig. 2. Specific regions for area averages are chosen where an ENSO response based on linear regression occurs. For each panel in Fig. 6, to visually assess temporal delay in response in local SST to the ENSO variability, time evolution of Niño 3.4 SST index is also shown.

Over the Indian Ocean the interannual variability in observed SSTs has a large contribution from the ENSO variability as is evidenced by good phase relationship between the observed and model simulated ensemble mean SST anomaly. The sign of response is also in phase with the sign of ENSO SST with warm (cold) ENSO events leading to a warming (cooling) in the Indian Ocean SSTs. The phase relationship, however, has a distinct delay with SST anomalies in the Indian Ocean lagging behind the ENSO variability in the tropical Pacific.

Over the western and North Pacific the phasing of ENSO related SST response is opposite to that over the Indian Ocean, and warm (cold) ENSO events result in cold (warm) SST anomalies. Further, the interannual SST variability is also not as tightly constrained by the ENSO as it was over the Indian Ocean, and this is likely because of the larger contribution from the atmospheric variability to the SST variability in extratropical ocean basins. There is also a delay in the response to the SST over the North Pacific relative to ENSO variability, but less so over the western



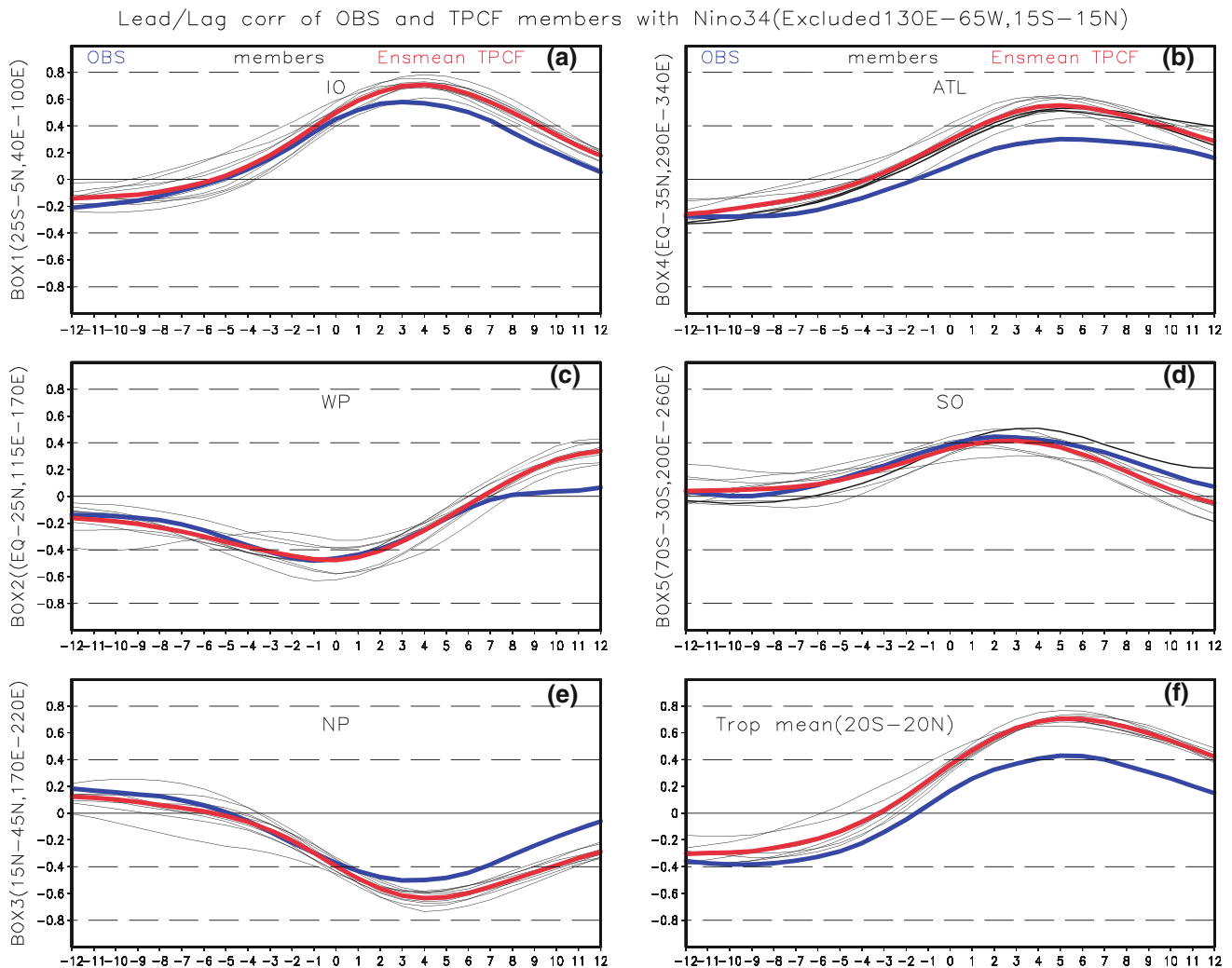


**Fig. 8** Lead-lag correlation between the SSTs area averaged over different ocean basins and Niño 3.4 SST index. **a** Indian Ocean; **b** Atlantic; **c** Western Pacific; **d** Southern Oceans; **e** North Pacific, and **f** tropical oceans. *Y* axis is for correlation and *x* axis is for lead/lag in

months. Niño 3.4 SST index lagging (leading) corresponds to negative (positive) integers. *Thick blue line* is correlation for observations; *thin black lines* are correlations for individual model simulations; *thick red line* is for correlation with ensemble mean

Pacific where variations seem almost in phase with the Niño 3.4 SST index.

Over the Atlantic and Southern Oceans, the phasing of the ENSO related SST variability becomes similar to that over the Indian Ocean with warm (cold) ENSO events leading to a warming (cooling) over the respective ocean basins. Similar to the other ocean basins, a delay in response in SST is also evident. Finally, for completeness, the time series of observed SST and model simulated SST for the tropical ocean basins are also shown in Fig. 6 (bottom right), and repeats what is shown in Fig. 5.

The delay in ENSO response in SST over the different ocean basins is further analyzed based on lead/lag correlations with the Niño 3.4 SST index, and results, both for observations and for the model simulation are shown in Fig. 7. Correlation for the model simulations are computed

for individual members and then averaged over all nine runs.

Consistent with the delay in response seen in various time series in Fig. 6, correlations in other ocean basins generally maximize with ENSO leading SST variability in other ocean basins. The spatial pattern of the response for observations and for the model simulation is remarkably similar with a horseshoe pattern of negative correlation surrounding the positive correlation in the ENSO region of the equatorial tropical Pacific. This is likely because the atmospheric ENSO teleconnection pattern simulated by the model that mediates responses in SST in remote ocean basins to ENSO resembles well its observational counterparts (not shown). Positive correlations exist for Indian and Atlantic Ocean basins, and reach their peak amplitude after the peak phase of the ENSO.

**Fig. 9** (Top row) Maximum positive correlation between local SSTs and Niño 3.4 SST index for **a** observations, and **b** model simulations. (Bottom row) Same as for the top row but for minimum negative correlation. Maximum and minimum correlations are obtained based on lead-lag correlation at each grid point. Regions where the absolute value of minimum or maximum correlation is  $<0.3$  are not shown

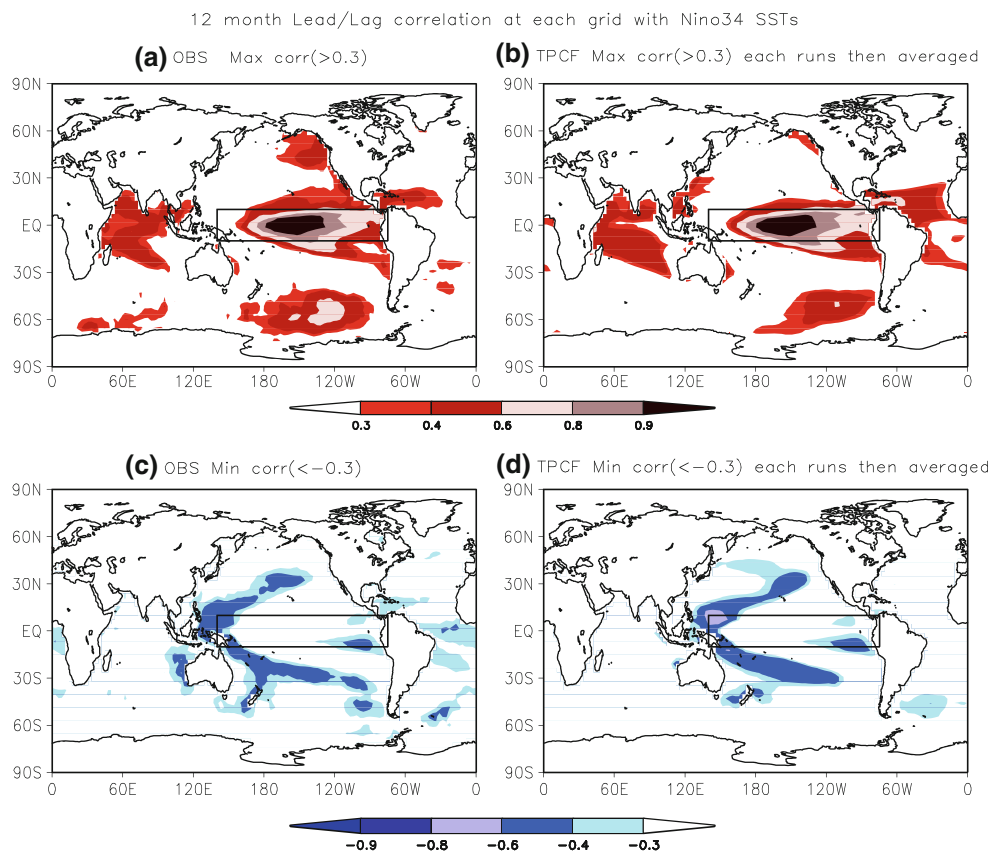
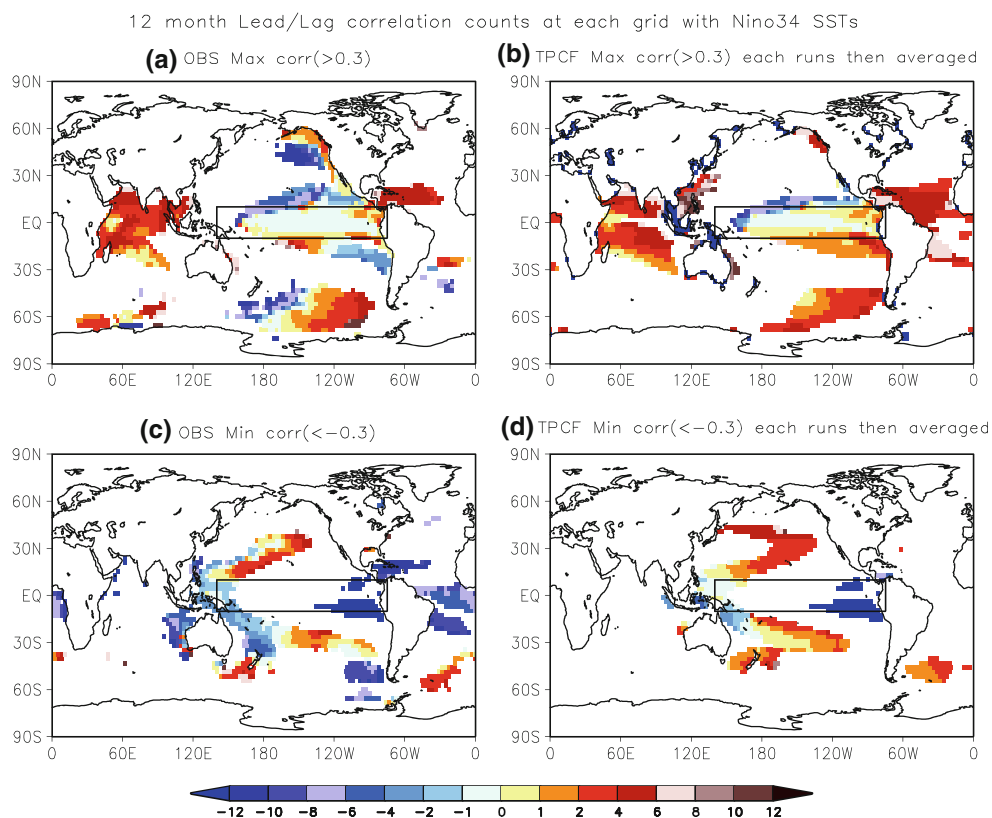


**Fig. 10** (Top row) Number of months at which the correlation between local SSTs and Niño 3.4 SST index is maximum positive for **a** observations, and **b** model simulations. (Bottom row) Number of months at which the correlation between local SSTs and Niño 3.4 SST index is minimum negative for **a** observations, and **b** model simulations. Positive (negative) values indicate Niño 3.4 SST index leading (lagging) local SST variability



The phase lag in the SST response in various ocean basins is quantified as lead/lag correlation between Niño 3.4 SST index and area averaged SST anomaly over the different boxes (Fig. 8). Lead/lag correlations are shown for observations (blue line), individual model simulations (thin black lines), and ensemble mean (red line). For all ocean basins, except in the western Pacific, the correlation maximizes with Niño 3.4 SST index leading by 3–4 months, and as discussed earlier the correlation is positive for area averages over the boxes in the Indian, Atlantic, and southern oceans, as well as for the tropics as a whole. The correlation is negative for the box averaged SST over the North Pacific. Overall the timing and the maximum amplitude of lead/lag correlation in the model simulation match well with those of the observations.

Based on the lead/lag correlations done on a data set with monthly resolution (Fig. 7), the maximum (or the minimum) value of correlation at each grid point is shown in Fig. 9. Similarly, the number of months of lead or lag at which correlations maximize is plotted in Fig. 10. Results are only shown over the regions where the absolute value of minimum or maximum correlation exceeds 0.3. The largest value of both maximum and minimum correlation is  $\sim 0.6$ , and for all these regions Niño 3.4 SST variability leads the SST variability in other ocean basins (Fig. 10). The general feature of ENSO SST variability leading is evident by the dominance of regions with red shading in Fig. 10 that correspond to ENSO SST leading. The analysis also provides a convenient way to summarize the time scale at which SSTs in other basins follow the ENSO SST variations, and confirms the results of Chen et al. (2008).

The physical reasons for the SST response in other ocean basins to ENSO variability in equatorial basins have been studied extensively. Given the slow time scale associated with oceanic pathways, the fundamental underpinning of the teleconnected response is via the atmospheric bridge, although the actual physics over different oceanic basins may differ. Various possibilities include a response in surface wind leading to a dynamical oceanic adjustment or via a thermodynamic adjustment due to changes in the latent heat (Lau and Nath 1996; Klein et al. 1999); remote response in precipitation (and associated cloudiness) via changes in the ascending and descending branches of the Hadley and Walker circulations leading to changes in the shortwave flux at the ocean surface (Fu et al. 1996); communication of ENSO SST anomalies via tropical atmospheric wave adjustment that leads to responses in tropical tropospheric temperature and surface specific humidity (Chiang and Sobel 2002) and their subsequent influence on the latent and sensible heat flux and SSTs (Klein et al. 1999).

## 4 Summary and discussion

Based on a novel design of coupled model simulations where SST variability in the equatorial tropical Pacific was constrained to follow the observed ENSO variability, and rest of the global oceans were free to evolve, ENSO responses in SSTs over the other ocean basins was analyzed. The unique features of the present analysis are summarized as follows.

- The analysis was not constrained by any a priori assumption, for example, linearity or assumptions fixing the lead/lag time scales between the teleconnected response.
- Because of the ensemble design of the model simulations, the analysis included signal-to-noise separation of SST variability. In the context of the SNR analysis, signal was due to the common ENSO variability that was included in all the simulations, and noise was the component that is internal to the coupled system and may be caused either by the internal variations in the oceans or variations in atmospheric variability leading to changes in the ocean.
- The analysis allowed us to discern the time scale of the oceanic response of SSTs in other ocean basins.

In a manner similar to the analysis of atmospheric climate variability forced because of ENSO, the present analysis followed the same approach but for SST variations in remote ocean basins. The design of experiments, and approach outlined herein, can also be utilized in attributing and understanding SST variability in different ocean basins to ENSO, and to quantify what fraction of variance in SST variability could be related to ENSO. The approach can also be utilized to remove the ENSO signal in surface temperature variations over the globe, and bring forth the contribution of other factors, such as changes in atmospheric composition and volcanic aerosols.

## References

- Alexander MA, Scott JD (2002) The influence of ENSO on air–sea interaction in the Atlantic. *Geophys Res Lett* 29. doi: [10.1029/2001GL014347](https://doi.org/10.1029/2001GL014347)
- Alexander MA, Bladé I, Newman M, Lanzante JR, Lau N-C, Scott JD (2002) The atmospheric bridge: the influence of ENSO teleconnections on air–sea interaction over the global oceans. *J Clim* 15:2205–2231
- Barnston AG (1994) Linear statistical short-term climate predictive skill in the Northern Hemisphere. *J Clim* 7:1513–1564
- Barnston AG, Chelliah M, Goldenberg SB (1997) Documentation of a highly ENSO-related SST region in the equatorial Pacific. *Atmos Ocean* 35:367–383

- Behringer DW, Xue Y (2004) Evaluation of the global ocean data assimilation system at NCEP: the Pacific Ocean. Preprints, Eighth Symposium on integrated observing and assimilation systems for atmosphere, oceans, and land surface, Seattle, WA, USA. Meteor. Soc. 2.3. Available online at [http://ams.confex.com/ams/84Annual/techprogram/paper\\_70720.htm](http://ams.confex.com/ams/84Annual/techprogram/paper_70720.htm)
- Chang P, Fang Y, Saravanan R, Ji L, Seidel H (2006) The cause of the fragile relationship between the Pacific El Niño and the Atlantic Niño. *Nature* 443:324–328
- Chen J, Del Genio AD, Carlson BE, Bosilovich MG (2008) The spatiotemporal structure of twentieth-century climate variations in observations and reanalyses. Part I: Longterm trend. *J Clim* 21:2611–2633
- Chen M, Wang W, Kumar A, Wang H, Jha B (2012) Ocean surface impacts on the seasonal-mean precipitation over the tropical Indian Ocean. *J Clim* 25:3566–3582
- Chiang JCH, Lintner BR (2005) Mechanisms of remote tropical surface warming during El Nino. *J Clim* 18:4130–4149
- Chiang JCH, Sobel AH (2002) Tropical tropospheric temperature variations caused by ENSO and their influence on the remote tropical climate. *J Clim* 15:2616–2631
- Compo GP, Sardeshmukh PD (2010) Removing ENSO-related variations from the climate record. *J Clim* 23:1957–1978
- Elliott JR, Jewson SP, Sutton RT (2001) The impact of the 1997/98 El Niño event on the Atlantic Ocean. *J Clim* 14:1069–1077
- England MH, Huang F (2005) On the interannual variability of the Indonesian through flow and its linkage with ENSO. *J Clim* 18:1435–1444
- Fu R, Liu WT, Dickinson RE (1996) Response of tropical clouds to the interannual variation of sea surface temperature. *J Clim* 9:616–634
- Goddard L, Graham NE (1999) The importance of the Indian Ocean for simulating precipitation anomalies over eastern and southern Africa. *J Geophys Res* 104:19099–19116
- Hoerling MP, Kumar A, Zhong M (1997) El Niño, La Nia and the nonlinearity of their teleconnections. *J Clim* 10:1769–1786
- Horel JD, Wallace JM (1981) Planetary scale atmospheric phenomena associated with the Southern Oscillation. *Mon Weather Rev* 109:813–829
- Huang B (2004) Remotely forced variability in the tropical Atlantic Ocean. *Clim Dyn* 23:133–152
- Huang B, Shukla J (2007) Mechanisms for the Interannual variability in the tropical Indian Ocean. Part II: Regional processes. *J Clim* 20:2937–2960
- Ji M, Kumar A, Leetmaa A (1994) Development of seasonal climate forecast system using coupled ocean–atmosphere model at National Meteorological Center. *Bull Am Meteorol Soc* 75:569–577
- Jones PD (1988) The influence of ENSO on global temperatures. *Clim Monit* 17:80–89
- Kanamitsu M, Ebisuzaki W, Woollen J, Yang S-K, Hnilo JJ, Fiorino M, Potter GL (2002) NCEP–DOE AMIP-II reanalysis (R-2). *Bull Am Meteorol Soc* 83:1631–1643
- Kelly PM, Jones PD (1996) Removal of the El Niño Southern Oscillation signal from the gridded surface air temperature data set. *J Geophys Res* 101:19013–19022
- Klein SA, Soden BJ, Lau N-C (1999) Remote sea surface temperature variations during ENSO: evidence for a tropical atmospheric bridge. *J Clim* 12:917–932
- Kumar A, Hoerling MP (1995) Prospects and limitations of seasonal atmospheric GCM predictions. *Bull Am Meteorol Soc* 76:335–345
- Kumar A, Hoerling MP (1997) Interpretation and implications of observed inter-El Niño variability. *J Clim* 10:83–91
- Kumar A, Hoerling MP (2000) Analysis of a conceptual model of seasonal climate variability and implications for seasonal predictions. *Bull Am Meteorol Soc* 81:255–264
- Kumar A, Hoerling MP (2003) The nature and causes for the delayed atmospheric response to El Nino. *J Clim* 16:1391–1403
- Kumar A, Yang F, Goddard L, Schubert S (2004) Differing trends in the tropical surface temperatures and precipitation over land and oceans. *J Clim* 17:653–664
- Kumar A, Jha B, L’Heureux M (2010) Are tropical SST trends changing the global teleconnection during La Niña? *Geophys Res Lett* 37:L12702. doi:10.1029/2010GL043394
- L’Heureux M, Collins D, Hu Z-Z (2013) Linear trends in sea surface temperature of the tropical Pacific Ocean and implications for the El Niño–Southern Oscillation. *Clim Dyn*. doi:10.1007/s00382-012-1331-2
- Lanzante JR (1996) Lag relationships involving tropical sea surface temperatures. *J Clim* 9:2568–2578
- Lau N-C, Nath MJ (1996) The role of the “atmospheric bridge” in linking tropical Pacific ENSO events to extratropical SST anomalies. *J Clim* 9:2036–2057
- Lau N-C, Nath MJ (2003) Atmosphere–ocean variations in the indopacific sector during ENSO episodes. *J Clim* 16:3–20
- McPhaden MJ, Busalacchi AJ, Anderson DLT (2010) A TOGA retrospective. *Oceanography* 23:86–103
- Moorthi S, Pan H-L, Caplan P (2001) Changes to the 2001 NCEP operational MRF/AVN global analysis/forecast system. *NWS Tech Proced Bull* 484:14. Available online at <http://www.nws.noaa.gov/om/tpb/484.htm>
- Newman M, Compo GP, Alexander MA (2003) ENSO forced variability of the Pacific decadal oscillation. *J Clim* 16:3853–3857
- Pacanowski RC, Griffies SM (1998) MOM 3.0 manual. NOAA/Geophysical Fluid Dynamics Laboratory, p 668
- Pan H-L, Mahrt L (1987) Interaction between soil hydrology and boundary layer developments. *Bound Layer Meteor* 38:185–202
- Peng P, Kumar A, Barnston AG, Goddard L (2000) Simulation skills of the SST-forced global climate variability of the NCEP-MRF9 and Scripps/MPI ECHAM3 models. *J Clim* 13:3657–3679
- Reynolds RW, Rayner NA, Smith TM, Stokes DC, Wang W (2002) An improved in situ and satellite SST analysis for climate. *J Clim* 15:1609–1625
- Rowell DP (1998) Assessing potential seasonal predictability with an ensemble of multidecadal GCM simulations. *J Clim* 11:109–120
- Saha S et al (2006) The NCEP climate forecast system. *J Clim* 19:3483–3517
- Stenchikov G, Delworth TH, Ramaseamy V, Stouffer RL, Wittenberg A, Zeng F (2009) Volcanic signals in oceans. *J Geophys Res* 114:D16104. doi:10.1029/2008JD011673
- Stockdale TN, Anderson DLT, Alves JOS, Balmaseda MA (1998) Global seasonal rainfall forecasts using a coupled ocean–atmosphere model. *Nature* 392:370–373
- Trenberth EK, Branstrator GW, Karoly D, Kumar A, Lau N-C, Ropelewski C (1998) Progress during TOGA in understanding and modeling global teleconnections associated with tropical sea surface temperatures. *J Geophys Res* 107(C7):14291–14324
- Xue Y et al (2012) A comparative analysis of upper ocean heat content variability from an ensemble of operational ocean reanalyses. *J Clim* 25:6905–6929